International Journal of Applied Earth Observations and Geoinformation 107 (2022) 102681

Contents lists available at ScienceDirect

International Journal of Applied Earth Observations and Geoinformation

journal homepage: www.elsevier.com/locate/jag

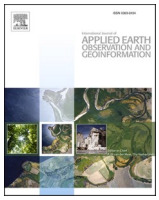

Combining spatial response features and machine learning classifiers for landslide susceptibility mapping

Ruilong Wei [a], Chengming Ye [a,*], Tianbo Sui [a], Yonggang Ge [b], Yao Li [b], Jonathan Li [c]

[a] Key Laboratory of Earth Exploration and Information Technology of Ministry of Education, Chengdu University of Technology, Chengdu 610059, China
[b] Institute of Mountain Hazards and Environment, Chinese Academy of Sciences, Chengdu 610041, China
[c] Department of Geography and Environmental Management, University of Waterloo, Waterloo, ON N2L 3G1, Canada

ARTICLE INFO

Keywords:
Landslide susceptibility
Feature fusion
Hybrid models
Machine learning

ABSTRACT

Reliable landslide susceptibility mapping (LSM) is essential for disaster prevention and mitigation. This study develops a deep learning framework that integrates spatial response features and machine learning classifiers (SR-ML). The method has three steps. First, depthwise separable convolution (DSC) extracts spatial features to prevent confusion of multi-factor features. Second, spatial pyramid pooling (SPP) extracts response features to obtain features under different scales. Third, the high-level features are fused into prepared ML classifiers for more effective feature classification. This framework effectively extracts and uses different-dimension features of samples, explores ML classifiers for beneficial feature classification, and breaks through the limitation of fixed input sample sizes. In the Yarlung Zangbo Grand Canyon region, data on 203 landslides and 11 conditioning factors were prepared for availability verification and LSM. The evaluation indicated that the area under the receiver operating characteristic curve (AUC) for the proposed SR and SR-ML achieved 0.920 and 0.910, which were 6.6% and 5.6% higher than the random forest (RF, with the highest AUC in ML group) method, respectively. Furthermore, the framework using 64 × 64 size inputs had the lowest mean error of 0.01, revealing that samples considering landslide scales could improve performance for LSM.

1. Introduction

Landslides are the gravitational movement of natural materials such as soil, debris, and rocks on a slope downwards (Hungr et al., 2014). They are ubiquitous in mountains and hills, frequently causing many casualties and severe economic losses. Further, its secondary hazards can cause sustained damage (Fan et al., 2019). Some studies (Gorum et al., 2011; Samia et al., 2016) have revealed that landslide evolution is controlled by complex environmental factors, such as topography, lithology, land cover, and hydrology. Driven by gravity, external triggers such as rainfall, earthquake, and human interference can lead to landslides. Therefore, it is essential to identify and predict the landslide spatial distribution to prevent and reduce potential damages.

In recent years, quantitative predictive methods, including physical and susceptibility assessment, have been introduced for regional landslide spatial prediction (Anagnostopoulos et al., 2015). Derived from slope stability and landslide formation, the physical models can produce reasonably accurate results through detailed geological field surveys (Jibson, 2011). However, numerous parameters are required for precise physical modeling, which is extremely hard to apply on a large scale (Bojadjieva et al., 2018). Recently, the development of the geographic information system (GIS) and remote sensing (RS) and research of landslide susceptibility mapping (LSM) have been used to analyze the potential correlations between the conditions of landslides and their probability (Achour and Pourghasemi, 2020; Huang et al., 2019; Tien Bui et al., 2016). Effectively, LSM can visualize landslide-prone areas and devise disaster prevention and mitigation strategies.

Currently, various quantitative methods have been introduced to aid LSM. Owing to the capability of effectively capturing the relationships between landslides and environmental conditions, machine learning (ML) is becoming widely applied in LSM, such as logistic regression (LGR) (Aditian et al., 2018), support vector machines (SVMs) (Marjanović et al., 2011), decision trees (DTs) (Xiao et al., 2018), and random forests (RFs) (Chen et al., 2018; Ye et al., 2021). However, most methods classify the samples directly but reveal few representative features from causative factors and landslides. Further, deep learning

* Corresponding author.
E-mail addresses: virylon@qq.com (R. Wei), rsgis@sina.com (C. Ye), suitianbo_9@live.com (T. Sui), gyg@imde.ac.cn (Y. Ge), yaoli@imde.ac.cn (Y. Li), junli@uwaterloo.ca (J. Li).

https://doi.org/10.1016/j.jag.2022.102681
Received 18 November 2021; Received in revised form 6 January 2022; Accepted 8 January 2022
Available online 19 January 2022

methods have become increasingly popular due to their ability to extract features, such as deep belief networks (DBNs) (Ye et al., 2019), recurrent neural networks (RNNs) (Thi Ngo et al., 2021), and convolutional neural networks (CNNs) (Wang et al., 2019). Among them, CNNs showed better performance on spatial feature extraction in the researches of LSM (Ghorbanzadeh et al., 2019b; Yang et al., 2021; Yi et al., 2020). However, limited by the data expression of landslide sampling, some architectures cannot be well applied to feature extraction.

Deep learning approaches, which can extract features and capture deep representations from massive data, have received considerable attention in LSM. However, only a few creative hybrid models were applied to the deep utilization of features (Chen et al., 2021; Fang et al., 2020; He et al., 2021). Most of the methods utilize only a single feature dimension and rarely consider multi-feature fusion, which leads to unacceptable generalization ability in complex scenes. Significantly, since the complex nonlinear correlation of factors and over-fitting, existing hybrid strategies take little advantage of each method for effective feature utilization.

To solve the problems mentioned above, it is essential to develop a more reliable strategy and explore its application in LSM. We proposed a deep learning framework that combines spatial response features and ML classifiers (SR-ML) for more accurate LSM. Our work offers three contributions. First, to obtain the spatial features and prevent confusion, depthwise separable convolution (DSC) was applied for complex factors. Second, to capture the robust response features and remove the limitation of fixed-size inputs, spatial pyramid pooling (SPP) was implemented for each factor under different scales. Third, to explore the effectiveness of high-level features that consider different dimensions, the ML classifiers were integrated to improve the performance of the framework for LSM. To assess the effectiveness of our SR-ML framework, we applied it to data for the Yarlung Zangbo Grand Canyon region. Several conventional methods, such as LGR, SVM, and RF, were used next for comparison. Also, we compared the ability of ML classifiers and full-connection (FC) layers on utilizing high-level features. Furthermore, we analyzed the influence of input sample sizes on model prediction.

2. Methods

2.1. Prediction framework

2.1.1. Samples construction

Traditional sampling methods use pixel or grid-based (Hussin et al., 2016), scarp (Clerici et al., 2006), and seed cell (Dagdelenler et al., 2016) to extract the statistical value of conditioning factors. Thus, the extracted data are a set of sequences in which one value represents a factor. Significantly, if landslide entities are converted to points, the landslide positioning techniques affect the final results (Pourghasemi et al., 2020). The pixel-based method extracts the attribute value of factors for ML models.

The quality of non-landslide is important to LSM models. Previous studies (Hu et al., 2020; Huang et al., 2017) review that there are mainly three sampling methods for non-landslide, i.e., random selection from landslide free areas (Pourghasemi and Rahmati, 2018), the seed cell procedure (Nefeslioglu et al., 2008), and acquisition from terrain area with low slope (Kavzoglu et al., 2014). The above methods subjectively select non-landslide samples, while the terrain units should be more considered under similar geomorphic environments.

Fig. 1 illustrates the process of sampling strategy. Unlike previous methods, we used square-shaped units to extract factor values as landslide and non-landslide samples, which had the same sampling size to maintain sample balance. The sub-watersheds were used as basic terrain units for sampling. Landslide and non-landslide samples should not be located in the same sub-watersheds. Specifically, landslide samples were determined by landslide inventory, non-landslide samples were randomly and evenly selected from the sub-watersheds without landslide evidence.

For analysis and modeling, the source data of factors are all converted to raster format with a spatial resolution of 12.5 m. This process was implemented by using ArcGIS Nearest Resample. An $n \times n$ pixel window is used to clip the factor raster, where n ranges from 4 to 128 due to the different scales of landslides. We used Geospatial Data Abstraction Library (GDAL) to clip the sample value of each factor under the same projection coordinate. These factor slices of the same size are stacked and regarded as multi-channel images; each channel represents a factor. Compared with the sequence, these samples are $11 \times n \times n$ matrices with more spatial and background information, which is conducive to extracting features by convolution.

2.1.2. Spatial response features and machine learning classifiers

The proposed framework of this study is based on DSC, SPP, fully connected (FC) layers, and ML classifiers. It can extract spatial and response features, which include the convolution features and pooling attribute features of multiple factors, respectively. Fig. 2 illustrates the model construction process, which has three parts: spatial response

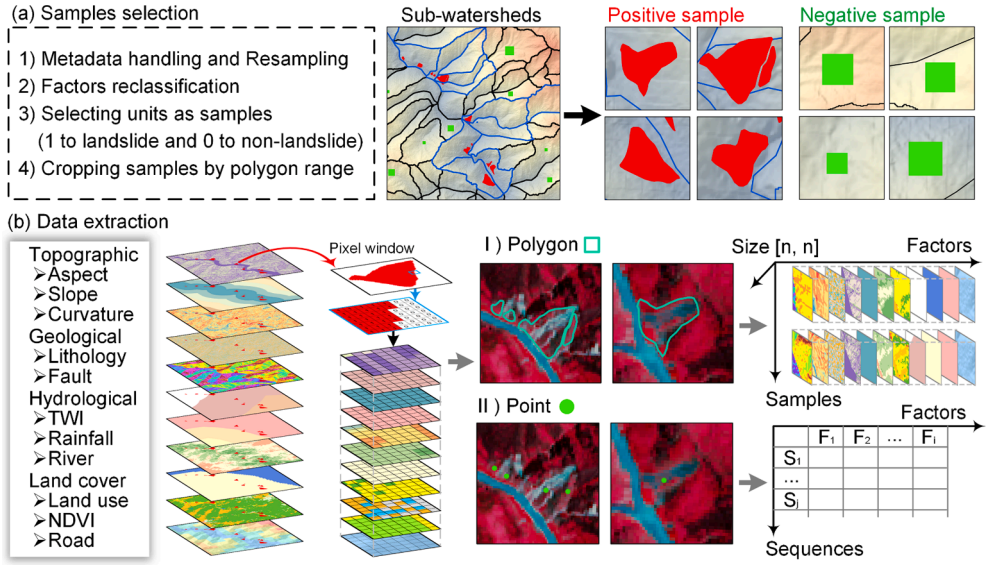

Fig. 1. Process of sample extraction. (a) Sample selection; (b) the differences in extracting data using square-shaped units and points.

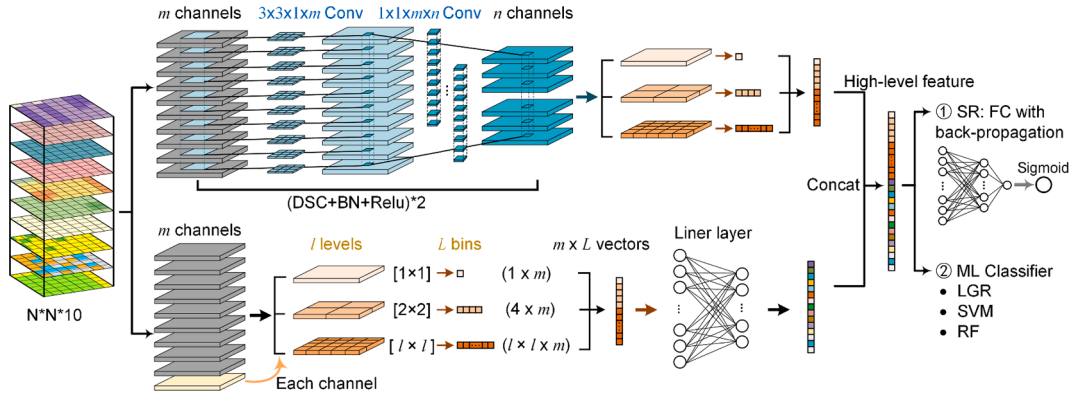

Fig. 2. The network structure of the spatial response features and the machine learning classifier.

feature extraction, feature fusion, and feature classification. For DSC, the mathematical expression can be written as

$$\overline{G}_{k,l,m} = \sum_{i,j} \overline{K}_{i,j,m} \cdot F_{k+i-1,l+j-1,m} \tag{1}$$

and

$$\dot{G}_{k,l,n} = \sum_{m} \dot{K}_{m,n} \cdot \overline{G}_{k-1,l-1,m} \tag{2}$$

where $\overline{K}$ is the depthwise convolution kernel of size $I \times J \times M$. The m th filter is used to produce the output feature map $\overline{G}$ in the m th channel. $\dot{K}$ is the pointwise convolution kernel of size $1 \times 1 \times M \times N$ that computes a new output $\dot{G}$.

For SPP, supposing a pyramid level of $a \times a$ bins, a feature map of $n \times n$, the pooling function includes kernel size $k = \lceil n/a \rceil$, stride $s = \lceil n/a \rceil$, and padding $p = \lfloor .(k \times a - n + 1)/2 \rfloor$. Here. $\lceil \cdot \rceil$ and $\lfloor \cdot \rfloor$ denote ceiling and floor operations. All pooled maps are concatenated into $m \times L$ dimensional vectors, where L denotes the number of all bins, and m is the number of input channels.

The output of the final FC layer is connected to a learning classifier, such as Sigmoid. The weights of the neural network can be optimized by back-propagation and gradient descent algorithms. The optimization is to minimize the loss value, which is calculated as:

$$\text{Loss} = -\frac{1}{m} \sum_{i=1}^{m} [y_i \log(\hat{y}_i) + (1 - y_i) \log(1 - \hat{y}_i)] \tag{3}$$

where m represents the number of input arrays, y_i and $\mathring{A}_{\cdot i}$ denotes the true and predicted value of the i th sample, respectively.

Spatial feature extraction. The DSC and SPP modules are used to extract spatial features. Considering the differences of spatial features between various factors, the DSC implements convolution for every single factor in the channel direction, preventing any confusion of multi-channel spatial features. Next, the pixel convolution in the depth direction extracts correlation features between factors (Chollet, 2017). Then, the feature maps are pooled by SPP bins to flatten multi-dimensional features into one-dimensional vectors. Finally, the pooled results of different pyramid levels are concatenated to obtain a multi-scale feature vector (Girshick, 2015).

Response feature extraction. The SPP module and liner layers are used to extract the response feature. Since artificially processed factors, such as Euclidean distance to rivers or roads, generally have less spatial information, the response feature reflects the attribute information between factors and landslide occurrence. The SPP processes input samples of different sizes with sparse pyramid levels to obtain multi-feature vectors under different scales (He et al., 2015). Then, the vector is transformed through a linear layer for feature combination (Lecun et al., 2015).

Feature fusion and classification. We employ a concatenation layer to combine spatial and response features to produce high-level features (Luong et al., 2015). Specifically, the above outputs are connected through vector space. In this study, we designed two strategies to use high-level features for classification. One is to pass the high-level features through two FC layers for nonlinear transformation. The sigmoid classifier can predict the probability of landslide occurrence, and the weights of the network can be updated by back-propagation and gradient descent. The other is to feed extracted high-level features into traditional ML models, including LGR, SVM, and RF. Then, the models predict the landslide probability by fitting features and labels.

2.1.3. Model construction

Fig. 3 shows the process of SR-ML framework construction and analysis. First, the values of factors were extracted from the landslide inventory and random non-landslides (203 landslides and 203 non-landslides). Previous researches (Hussin et al., 2016; Park and Lee, 2014; Pawluszek-Filipiak and Borkowski, 2020) have studied the effect of train-test split ratio on the model, indicating that a similar ratio of training and testing dataset has a favorable predictive ability. To obtain a robust prediction model, the sample dataset was randomly divided into training (50%) and testing (50%). Second, collinearity analysis and importance analysis methods were executed to evaluate the rationality of the factors. Third, the SR-ML, SR, and other ML models were constructed in producing the LSMs. Finally, the performance of the applied modules, namely DSC and SPP was discussed by accuracy measures, and the influence of sample size on the model was also analyzed.

2.2. Evaluation methods

2.2.1. Factor analysis

The frequency ratio (FR) represents the correlation between landslide occurrence and each causative factor in different classification intervals (Lee and Pradhan, 2006). The area with FR exceeding 1 has a higher correlation to landslide occurrences (Achour et al., 2018; Aditian et al., 2018). FR formula can be written as

$$\text{FR} = \frac{N_{ij}/A_{ij}}{N_r/A_r}, \tag{4}$$

where N_{ij} is the number of landslides in subclass j of the i th factor. A_{ij} is the area associated with the subclass j of the i th factor. N_r is the total number of landslides, and A_r is the total area of study.

The variance inflation factor (VIF) and tolerance (TOL) can quantify the multicollinearity among the factors (Arabameri et al., 2020). Collinearity means a high correlation between two or more factors, which are not independent of each other (Wang et al., 2019). TOL and VIF formulas can be written as

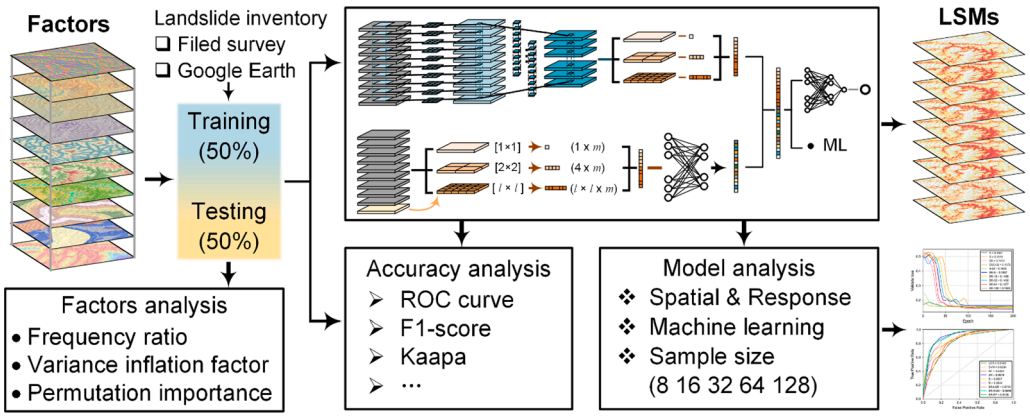

Fig. 3. Flowchart of the model's construction and analysis.

$$TOL = 1 - R_j^2 \tag{5}$$

and

$$VIF = 1/TOL \tag{6}$$

where R_j^2 denotes the coefficient of determination for the regression of explanatory j on all the other interpretable variables. VIF > 10 or TOL < 0.1 indicates a multi-collinearity problem and corresponding factors should be removed (Tien Bui et al., 2016).

The permutation importance (PI) can represent the contribution of features to a particular model. It is calculated by the accuracy decline between the original metric and disrupted metric in the specified feature column (Huang et al., 2016). The higher PI value of the factor means more contribution to landslide occurrence. PI formula can be written as

$$i_j = s - \frac{1}{K}\sum_{k=1}^{K} s_{k,j} \tag{7}$$

where i_j is the importance of the feature j, s is the accuracy score calculated from the original data, K is the number of iterations, and $s_{k,j}$ is the score calculated from corrupted data that randomly shuffle column j.

2.2.2. Accuracy analysis

The statistical evaluation measures are used to validate the performance of the trained models. This study chose overall accuracy (OA), Precision, Recall, Sensitivity, Specificity, F1-score, and Kappa to evaluate the constructed models (Huang et al., 2020). Kappa can indicate the reliability of classification models.

Moreover, we also used the receiver operating characteristic curve (ROC) to measure classification performance, this curve is plotted by two statistical values (false positive and true positive) with various cut-off thresholds, and the area under the ROC (AUC) is used to evaluate the accuracy of the model quantitatively (Park and Kim, 2019).

3. Materials

3.1. Study area

The study area (18000 km^2) is located on the eastern Himalayan syntaxis, with geographic coordinates of 94.45°–95.83° E and 29.19°–30.52° N (Fig. 4). This region is part of Nyingchi, Tibet Autonomous Region, and located in the Namcha Barwa tectonic node of the Himalayan suture zone, also known as the Grand Canyon region of the Yarlung Zangbo River.

Geologically, this region is surrounded by the Lhasa Block, which consists of low- to medium- metamorphic metasedimentary rocks, granite zones, layered gneiss intervals, and Gangdese plutons (Z. Li et al., 2021). The topography mainly consists of deep-cut valleys, and the elevation ranges from 324 m to 7782 m (Mount Namcha Barwa). High mountains collide with water vapor from the Indian Ocean Monsoon, creating rainy weather from May to September (Ma et al.,

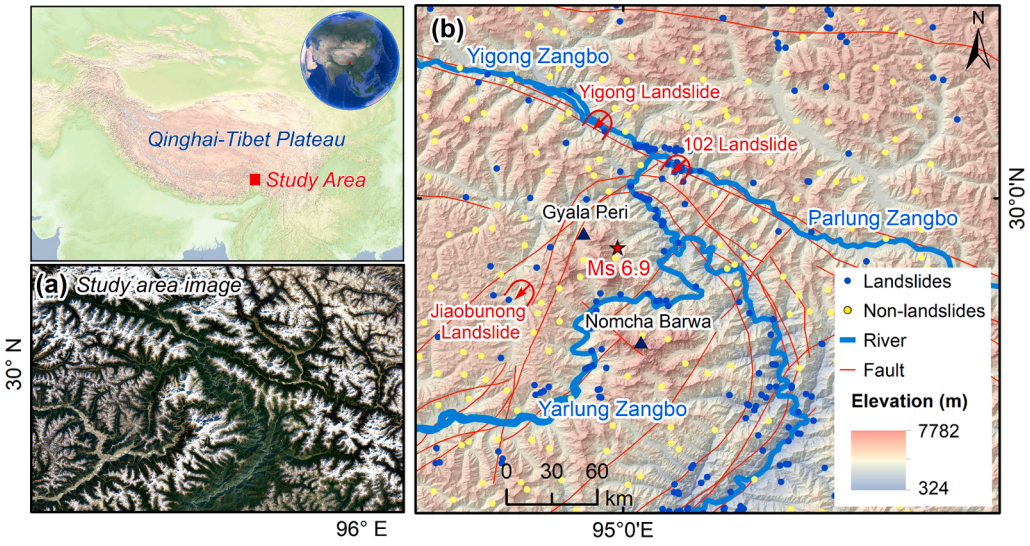

Fig. 4. Landslide inventory map and remote sensing image of the study area.

2020) and widespread glaciers. The global temperature rise leads to regional glacial melting and avalanches (C. Chen et al., 2020). Owing to the complex topography, geology, and hydrology, landslides occur frequently under precipitation and earthquake.

3.2. Landslide inventory

The landslide inventory records the spatial position, geometry, material, and movement types of landslides. In this study, the inventory consists of 203 landslides collected from remote sensing image interpretation, field surveys, and the Land and Resources Department of Sichuan Province. Referring to reference (Hungr et al., 2014), the movement types of landslides are divided into four categories: fall, slide, flow, and spread. Fig. 5 shows a graphic illustration for different landslide types with the corresponding sample images. The recorded landslides are mainly the sliding type and soil material, with areas ranging from 400 m^2 to 3×10^7 m^2. These landslides are mainly caused by natural factors such as seasonal heavy rainfall and earthquakes and are distributed near rivers and valleys. Over the years, landslides have caused catastrophic damage in this area. On April 09, 2000, a large-scale rock avalanche dammed the Yigong Zangpo River, forming an extensive rockslide-dammed lake (Delaney and Evans, 2015; Zhou et al., 2016). On November 18, 2017, a magnitude Ms. 6.9 (Mw 6.4) earthquake struck the east Himalayan syntaxis, located in the Nyingchi, triggered at least 1816 landslides and 3 dammed lakes (Zhao et al., 2021, 2019).

3.3. Landslide conditioning factors

Referring to the prior research, literature, and field surveys (Chen et al., 2017a; Du et al., 2019; Wang et al., 2020; Xu et al., 2009), we chose 11 influential conditioning factors, which reflect various features of landslide (Fig. 6). The datasets of factors were collected from free network resources, government websites, and Google Earth Engine (GEE). Table 1 details the sources and scales of these factors. These factors are processed as explanatory variables to describe the properties of the landslide. The distance parameters, namely rivers, roads, and faults, were calculated using the Euclidean distance. For continuous factors, the Jenks natural break method was applied to determine the threshold values of the subclasses.

Topographical factors are extracted through spatial analysis of the digital elevation model (DEM) (Fan et al., 2019; Gorum et al., 2011; Guzzetti et al., 2012). Since hillsides receive solar radiation and rainfall, the aspect regulates moisture movement and soil properties (Sameen et al., 2020). As the slope increases, the shear stress within the soil or unconsolidated sediment generally increases (Guo et al., 2015). Curvature affects the velocity of water flow and erosion (Sharma and Mahajan, 2019), and it is classified as concave (<-0.1), planar (-0.1 to 0.1), or convex (>0.1).

Hydrological factors affect landslide occurrence arising from the surface water process. The topographic wetness index (TWI) indicates the conditions of soil, geography, and runoff volume (He et al., 2019). Rivers can erode slopes or lower parts of saturated materials with fluctuating river water, thus negatively affecting stability (Zhang et al., 2019). Rainfall is an important external factor leading to landslides (Guo et al., 2021).

Land cover factors influence the mechanical properties and hydrological environment of the soil. The normalized difference vegetation index (NDVI) quantifies vegetation growth and the coverage of slope surfaces (Yunus et al., 2020). Land use from human activity is an important factor in slope instability. Different land types influence the soil's mechanical properties and hydrological environment (Huang et al., 2019). The roads are considered an important anthropogenic factor for triggering landslides (Chen et al., 2017b). Areas with slope cuts for road construction are susceptible to landslides.

Geological factors affect the strength and permeability of rock and soils. The lithology of the study area was divided into five categories, from soft to hard. Faults are highly susceptible to landslides because the weak structural plane leads to rock body rupture and weathering, which often intensifies the occurrence of landslides (Xiao et al., 2018).

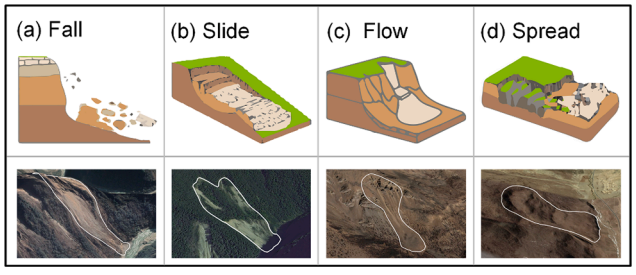

Fig. 5. Movement types of the landslide and the corresponding samples (Varnes, 1978).

4. Results

4.1. Significant conditioning factors

Table 2 illustrates the result of collinearity and importance analysis for each conditioning factor. The higher VIF value of the factor means probable multicollinearity with others (Hong et al., 2015). The VIF and TOL values of our work were in the critical range of collinearity. After the model construction, the PI value was used to quantify the influences of factors on landslide evolution. The result shows that NDVI, slopes, rainfall, and rivers are the four most important factors for landslide occurrence in the study area. Referring to previous studies in this region (Wu et al., 2021; Zhao et al., 2021, 2019), the slope of this area is steeper than other areas in Tibet. Frequent geological activities and river erosion have also had an impact on the occurrence of landslides.

Fig. 7 shows the percentage distribution and FR values for the factors subclass. A high FR indicates a strong relationship between landslide probability and the specified attribute interval (Dao et al., 2020). Referring to the previous study (Z. Li et al., 2021; Zhao et al., 2019), for distance parameters, the areas close to the river, road, and fault have a high FR value, which indicates that landslide occurrence has a spatial correlation with these factors. For topographical factors, landslides are likely to occur on the slopes with 30°–50°and facing southwest and south. The more abundant rainfall has the higher FR value, indicating an increased probability of landslide occurrence. For lithology, the soft layers are relatively more prone to landslides. For land cover, landslides are more distributed in bare land. Owing to glaciers in the study area, the landslides are mainly located on the slopes with lower elevation, vegetation growth, and close to rivers. These areas have higher NDVI values. The melting of glaciers caused by the temperature rise may also be the reason for landslide occurrence. Referring to PI results, the FR changes of important factors have a tendency and obvious response to landslide occurrence.

4.2. Landslide susceptibility maps (LSMs)

For better visualization, the LSMs were drawn using Inverse Distance Weighted interpolation and Jenks natural break method in Arcpy. Fig. 8 shows the LSMs generated by the five models, divided into five levels: very low, low, moderate, high, and very high susceptibility. The standard deviation and Min-Max for the proportion of five levels were 1.44 (28.95, 32.71), 2.62 (18.96, 26.37), 2.89 (17.26, 25.37), 1.22 (14.11, 17.67), and 1.86 (8.7, 13.36), respectively. The result shows that the prediction performance of the models is different in low and moderate susceptibility areas and similar in those of high susceptibility. The LSM results are consistent with previous studies in this region (Du et al., 2019; Wu et al., 2021). Historical landslides are distributed in high and very high susceptibility areas, which indicates the rationality of the

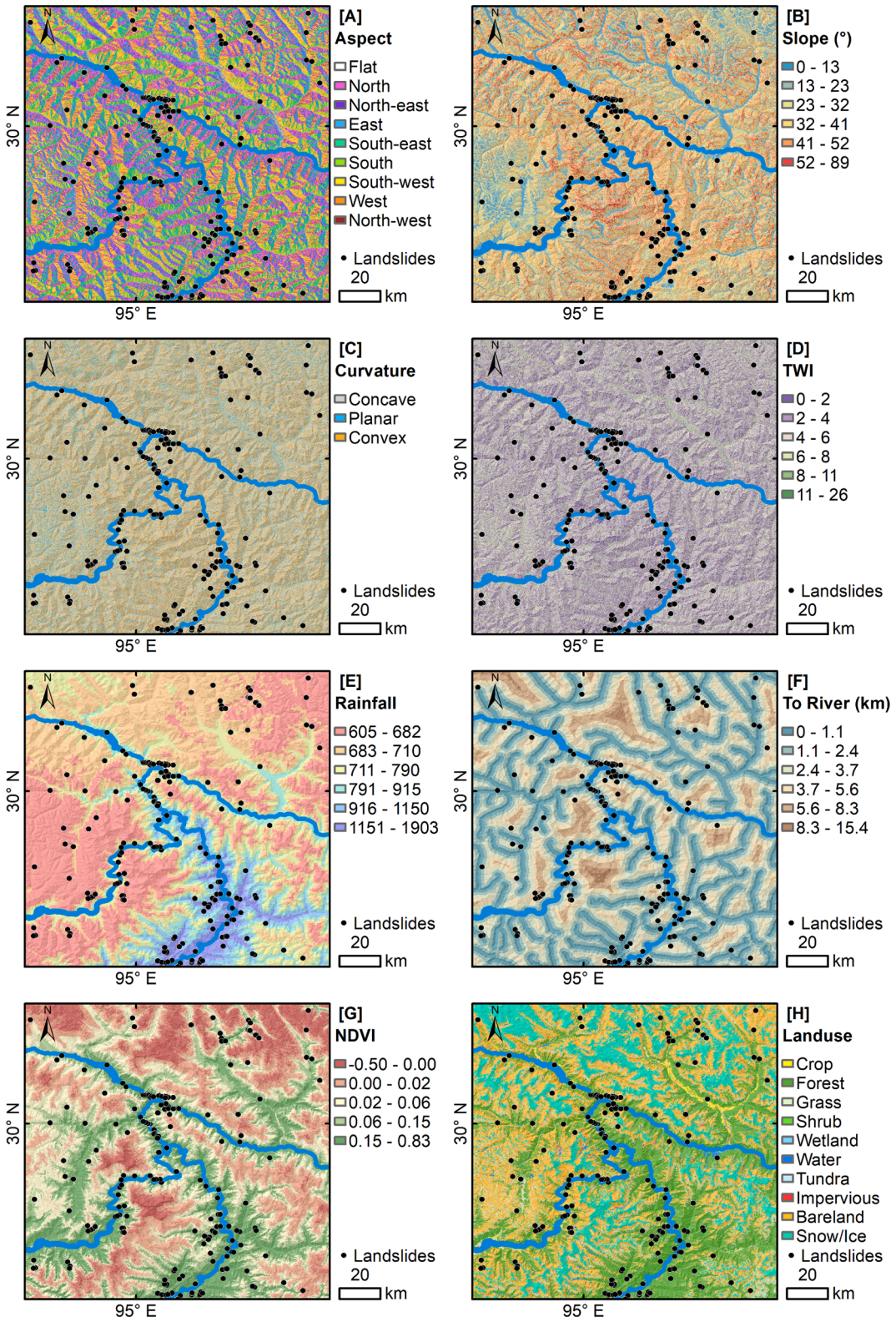

Fig. 6. Landslide conditioning factors. (a) Aspect, (b) slope, (c) curvature, (d) TWI, (e) rainfall, (f) distance to river, (g) NDVI, (h) land use, (i) distance to road, (j) lithology, and (k) distance to fault.

generated LSMs. Spatially, the areas with a high probability of landslide occurrence are mainly located near canyons and rivers. Geologically, these areas have loose lithology and many active faults.

Fig. 9 shows the satellite image and LSMs of the Yigong landslide. The sliding mass rushed at high speed into the river, heaping up a landslide dam. We selected this area to evaluate the sensitivity and reliability of models. It can be seen that SR and SR-RF predicted the source and deposit areas as high landslide probability. The ML models

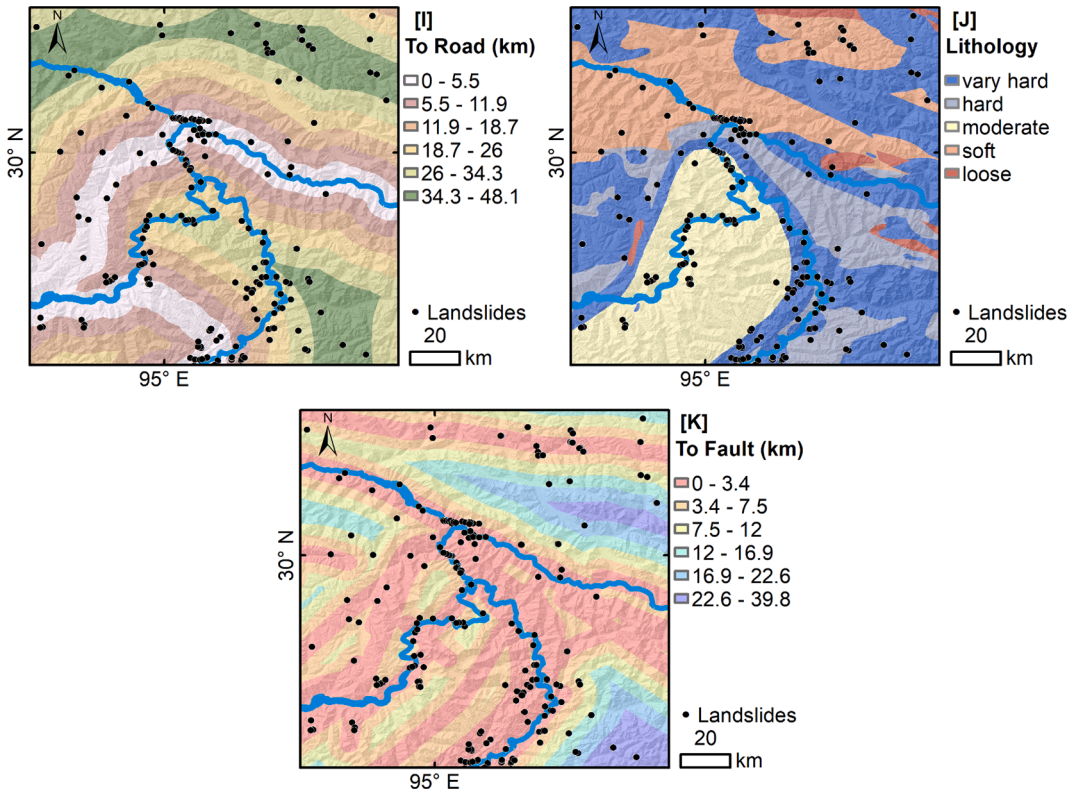

Fig. 6. (*continued*).

Table 1
The data sources of factors used in this study.

Factors	Data (Resolution/ Scales)	Type	Data Sources
Topography	ALOS DEM (12.5 m)	Raster	Alaska Satellite Facility (https://vertex.daac.asf.alaska.edu)
TWI	ALOS DEM (12.5 m)	Raster	Alaska Satellite Facility (https://vertex.daac.asf.alaska.edu)
Land use	FROM-GLC10 (10 m)	Raster	Global Land Cover (http://data.ess.tsinghua.edu.cn)
NDVI	Landsat 8 8-Day NDVI Composite (30 m)	Raster	Google Earth Engine Data (https://developers.google.com/earth-engine/datasets)
Road	Third pole road dataset (1:1000,000)	Polyline	National Tibetan Plateau Data Center (http://data.tpdc.ac.cn)
Rainfall	Data set of annual rainfall in Tibet (1000 m)	Raster	National Tibetan Plateau Data Center (http://data.tpdc.ac.cn)
River	Basic Geographic Information Data of China (1:1000,000)	Polyline	National Geomatics Center of China (http://ngcc.sbsm.gov.cn/ngcc)
Lithology	The National Geological Map Spatial Database (1:1000,000)	Polygon	Geoscientific Data & Discovery Publishing Center (http://geodb.cgs.gov.cn/)
Fault	Chinese active tectonic spatial database (1:4,000,000)	Polyline	National Earthquake Data Center (http://data.earthquake.cn)

predicted source areas as a low or moderate probability. The results indicate that our proposed model is more reasonable and reliable in producing LSMs, which can improve the accuracy of hazard prediction.

Table 2
Landslide conditioning factor analysis.

Factors	Collinearity		Importance
	VIF	TOL	PI
Aspect	1.054	0.949	0.012
Slope	1.112	0.900	0.037
Curvature	1.016	0.984	0.001
TWI	1.084	0.923	0.002
Rainfall	1.797	0.557	0.034
Distance to river	1.441	0.694	0.024
NDVI	**2.624**	**0.381**	**0.082**
Land use	1.787	0.560	0.009
Distance to road	1.318	0.759	0.005
Lithology	1.138	0.879	0.001
Distance to fault	1.296	0.771	0.021

4.3. Model parameters

We used grid search to find the optimal hyper-parameters of the ML models and SR models. All methods were implemented in Python using Scikit-learn and Pytorch. Owing to the finite number of parameters, LGR is suitable for generating baseline models in prediction analysis for the contrastive ML models. The LibLinear was set as the optimization method. SVM is a non-parametric supervised algorithm by splitting hyperplane in the feature space. The kernel function was RBF, and the C value was 6, which controls the fitting effect of the model. RF is a supervised classification method that ensembles decision trees. The numbers and maximum depth of trees in the forest were 300 and 8, respectively, whereas large parameters may cause over-fitting.

For our proposed SR model, we trained and tested the model for a total of 200 epochs. The batch size for fixed-size and variable-size input were 16 and 1, respectively. In the training process, we used the reduction scheduler that learning rates from 0.01 to 0.0001. The optimizer and activation function were Adaptive Moment Estimation

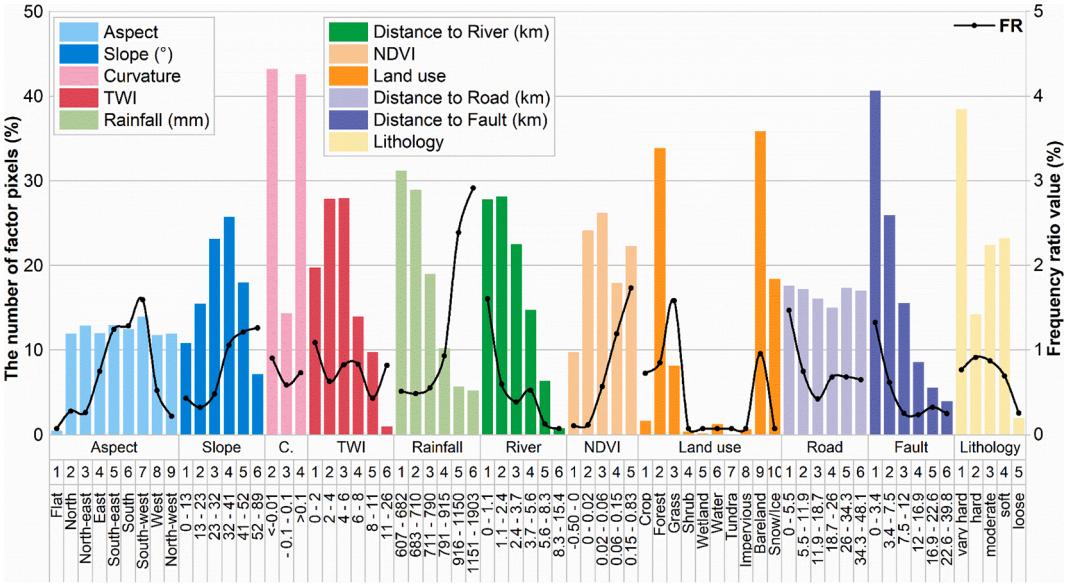

Fig. 7. Relationship between landslides and the conditioning factors.

(Adam) and Rectified Linear Unit (ReLu), respectively. The details of the SR model construction were described in Section 2.1. In DSC, the number of filters was set as 30. For SPP, the spatial pyramid levels for features extraction were set as [1, 4, 16] by controlled fine-tuning.

4.4. Model comparison

Table 3 and Fig. 10 show the quantitative evaluation results of LSM models in the testing dataset. SR-ML was highly accurate, especially the SR-RF, which achieved the best landslide predictive ability with the highest AUC (0.920) and OA (0.852). Compared with benchmark ML models, SR-ML achieved satisfactory accuracy results. Also, SR-ML models were better than SR, and the results showed the superiority of the ML classifier. While SR-LGR (0.903 of AUC) and LGR (0.837 of AUC) had the worst predictive performance in their groups, SR-LGR was even worse than SR, and it showed inferiority of generalized linear model in the fitting of complex correlation between landslide and factors. Besides, SR-ML group models have the highest Specificity value (0.922), which can accurately classify non-landslide areas as stable slopes, SR group models have the highest Sensitivity value (0.862), which can correctly identify landslide-prone areas to provide safe mitigation guidance.

To explain why the SR model has advantages in feature extraction, we conducted several comparative experiments with S and R. The loss curve in the testing process is shown in Fig. 10, reflecting the model's predictive ability. Specifically, the AUC of S (0.907) and R (0.908) were slightly worse than SR (0.910), which indicated that features fusion could improve the prediction ability. Both S and R were better than RF (0.854) of the best ML model, which illustrated that extracted spatial response features can identify landslides from input data. In addition, for spatial feature, the loss curve demonstrated that S, S-32, and DSC-32 had low loss values, which shows the sensitivity of the convolution feature to landslide identification.

The statistically significant differences between the LSM models were investigated using the Wilcoxon signed-rank test. When z-value exceeds critical values of (–1.96 to +1.96) and the p-value < 0.05, the null hypothesis will be rejected and there is a significant difference between the performance of models (Tien Bui et al., 2016). Table 4 shows the results of the statistical significance test for pairwise comparisons of the models. Except for the LGR and SVM (z-value = –1.815, p-value = 0.07), other models performed differently from each other in LSM.

5. Discussion

5.1. High-level feature representation

Landslide evolution is controlled by numerous predisposing factors (Guo et al., 2015). Deep learning can fit the complex relationship between environmental factors and landslide occurrence, and extract high-level features (Y. Li et al., 2021; Ye et al., 2019). Previous studies have proved that convolution is effective in LSM applications (Y. Chen et al., 2020; Sameen et al., 2020; Wang et al., 2019), but the factor attribute is also worth considering because distance parameters, such as roads, lack spatial information. Some recent researches showed the potential of deep learning in feature extraction (Lei et al., 2019; Thi Ngo et al., 2021; Wei et al., 2021). In our research, convolution features and factor attributes were extracted and combined as high-level features that feed into ML classifiers for LSM. Spatial features and response features focus on different dimensions or directions of samples, which is similar to the attention mechanism in image classification (Ji et al., 2020).

In our experiment, based on factor images, the neighborhood spatial information is extracted by DSC layers, and the factor attribute under different receptive fields are extracted by multi-scale pooling layers. This is different from the general pixel-based method to form a sequence by factor attributes. Fig. 11a illustrates the features extraction process from the multi-channel image of factors. Fig. 11b is a visualization of the high-level features of 203×3003 generated from SPP. It can be seen that spatial response features have various distributions in landslide and non-landslide modes. As shown in Table 3, the two kinds of features are fused and integrated into the proposed model, distinguishing landslides more effectively.

5.2. Influence of sample size

Unlike the pixel-based sampling of predisposing factors, the sample size is an important parameter of the convolution model. Owing to the limitation of FC layers, convolution models can accept fixed-size samples. Some researchers explored the impact of sample size on landslide models (Ghorbanzadeh et al., 2019a; Yi et al., 2020). The proposed framework can accommodate different sizes of input samples. However, for spatial features, the smaller sample size contains less information closing to pixel-based sampling, and a large sample size will cause bias and redundancy. Therefore, it is necessary to explore the influence of sample size on the model's ability to extract high-level features.

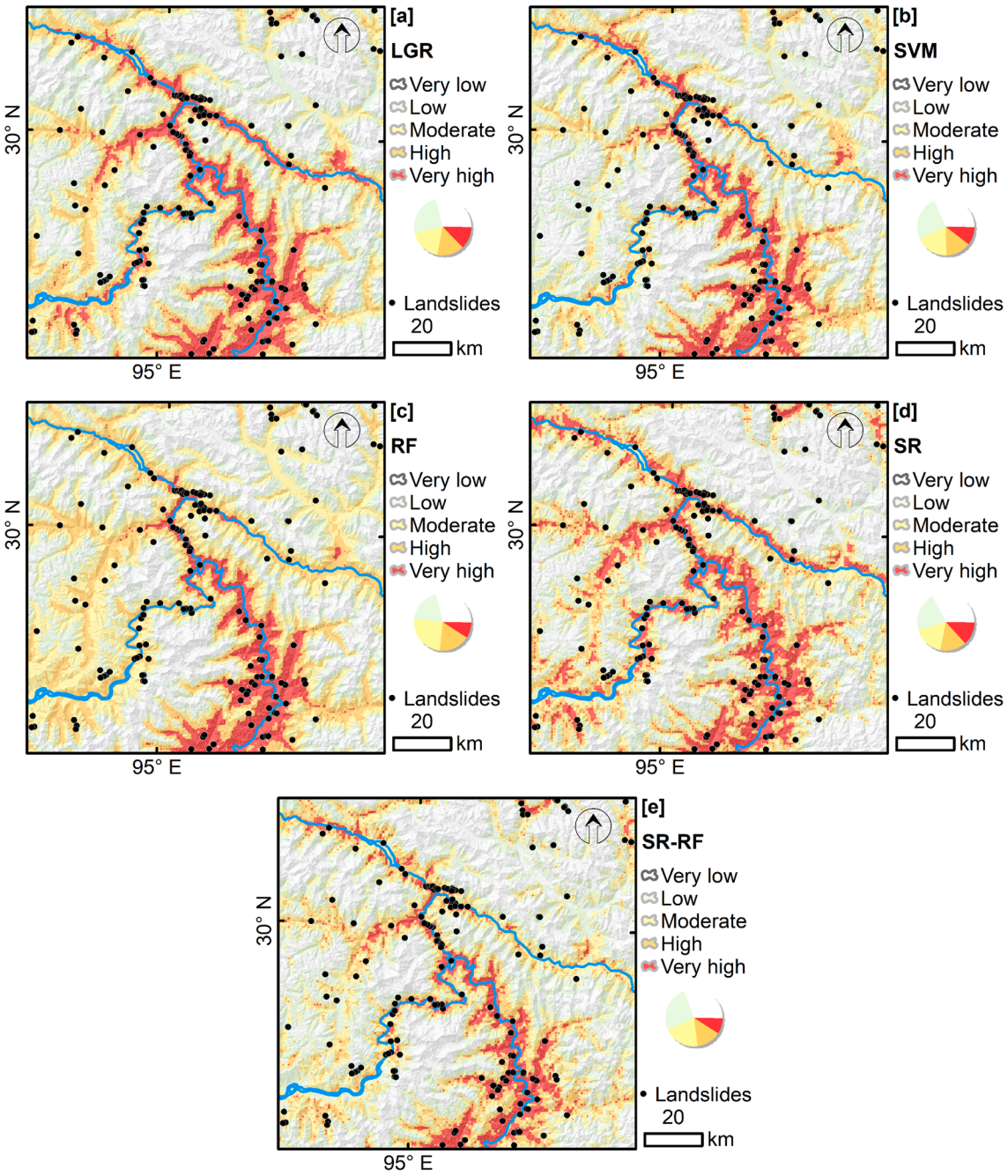

Fig. 8. LSMs produced by (a) LGR, (b) SVM, (c) RF, (d) SR, and (e) SR-RF.

We sliced different sizes of patches based on sample points for testing and comparison. Referring to the scales of landslides in the study area, the sample size ranges from 8 to 128. Fig. 10 illustrates the loss curve under different sizes of input samples. When the size is 64 × 64, the SR model reached the lowest loss value (0.1376). This phenomenon can guide us to set the pooling levels. In practical experiments, the model had a similar ability when using input samples with sizes of 64 and 32. To reduce the parameters of the model, we chose 16 as the maximum pool level to implement 2 × 2 pooling in each bin.

To further explore the relationship between samples and the model prediction ability, we analyzed the landslide scale and the corresponding sample size in the study area and then calculated the error between model predicted values and the true values under different sizes of input samples (Fig. 12). It can be observed that most of the landslides are small, with sample sizes ranging from 16 to 64, and the model has lower mean errors (0.01 lowest) in this interval. This phenomenon can be explained by the samples in this interval having relatively complete information. The model can extract high-level features at a suitable scale effectively (Chen et al., 2021), thus performing better prediction ability.

5.3. Performance of framework

Accurate LSM is essential for disaster prevention and mitigation. Therefore, it is of great significance to develop a more reliable framework and explore its application in LSM. Owing to the complex factors (Jia et al., 2019; Zhao et al., 2021), landslides occur frequently in our study area. Previous researches in this region (Du et al., 2019; Wu et al., 2021) using statistical and expert methods have yielded suitable results, which were similar to our LSMs. However, these conventional models can hardly in extracting high-level feature representation and further

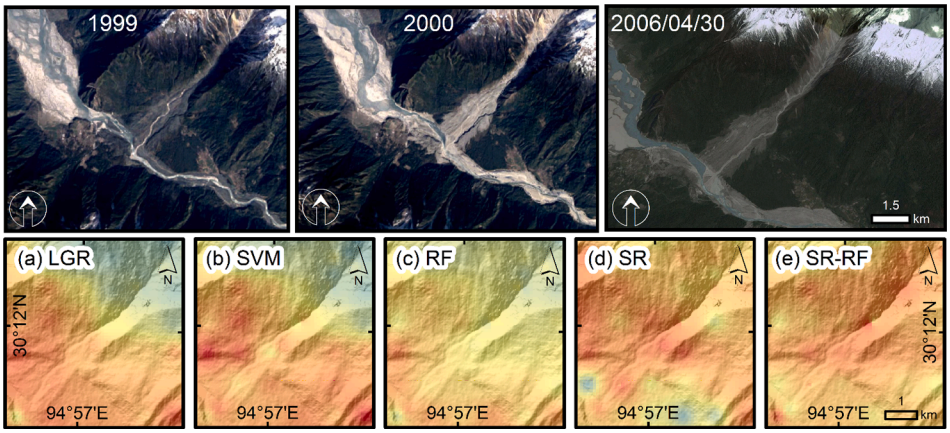

Fig. 9. The Google earth image of the Yigong landslide and the detailed display of five LSMs: (a) LGR, (b) SVM, (c) RF, (d) SR, and (e) SR-RF.

Table 3
Prediction capability of LSM models based on testing dataset.

LSM Models		TP	TN	FP	FN	AUC	OA	Pre	Rec	Sen	Spe	F1	Kappa
ML	LGR	77	78	24	24	0.837	0.764	0.762	0.762	0.762	0.765	0.762	0.527
	SVM	76	82	20	25	0.843	0.778	0.792	0.752	0.752	0.804	0.772	0.557
	RF	81	77	25	20	0.854	0.778	0.764	0.802	0.802	0.755	0.783	0.557
SR	S	94	70	31	8	0.907	0.808	0.752	0.922	0.922	0.693	0.828	0.615
	R	95	78	20	10	0.908	0.852	0.826	0.905	0.905	0.796	0.864	0.703
	SR	87	85	20	11	0.910	0.847	0.813	0.888	0.888	0.810	0.849	0.695
SR-ML	SR-LGR	89	81	13	20	0.903	0.837	0.873	0.817	0.817	0.862	0.844	0.675
	SR-SVM	86	80	14	23	0.915	0.818	0.860	0.789	0.789	0.851	0.823	0.636
	SR-RF	95	78	16	14	0.920	0.852	0.856	0.872	0.872	0.830	0.864	0.702

True positive (**TP**) denotes the number of landslides correctly identified, true negative (**TN**) denotes the number of non-landslides correctly classified, false positive (**FP**) refers to the number of samples incorrectly predicted as non-landslides, false negative (**FN**) refers to the number of incorrect predictions that should be landslides. **Pre**: precision, **Rec**: recall, **Sen**: sensitivity, **Spe**: specificity, **F1**: F1-score.

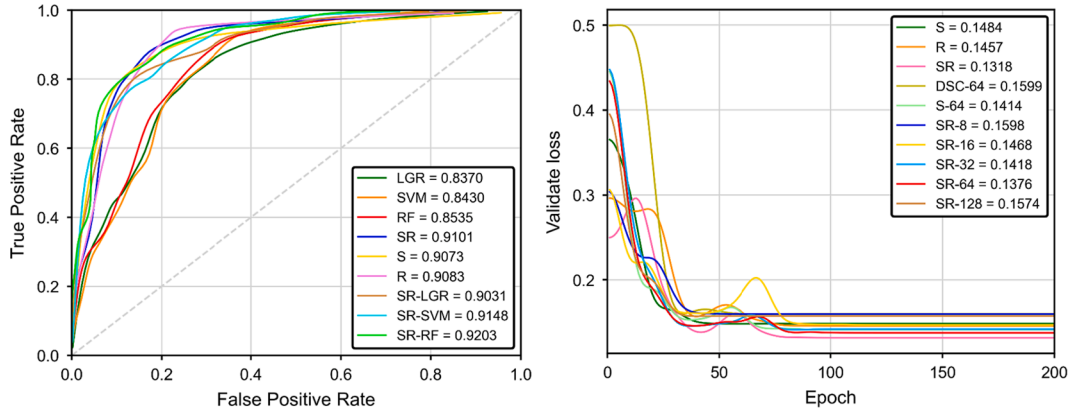

Fig. 10. Left: ROC curve of different LSM models based on the testing dataset. Right: Loss values of models testing process.

Table 4
Pairwise comparison of the five models.

	LGR vs.				SVM vs.			RF vs.		SR vs.
	SVM	RF	SR	SR-RF	RF	SR	SR-RF	SR	SR-RF	SR-RF
z-value	–1.815	–2.400	5.205	9.020	–5.936	2.531	7.047	5.241	15.804	3.278
p-value	0.070	0.016	0.000	0.000	0.000	0.006	0.000	0.000	0.000	0.001

exploring the inherent relationship of factors. In previous studies (He et al., 2021; Yang et al., 2021), it has been confirmed that spatial feature extraction by convolution and feature fusion can improve the prediction accuracy, but ML models are generally used for control experiments, and the extracted high-level features lack deeper application. Some studies (Fang et al., 2020; Pham et al., 2017) proved the superiority of hybrid models by reducing the variance and bias. This research aims to develop a hybrid framework, in which deep learning methods are for feature extraction and ML classifiers are for prediction.

Compared with the black box operation of feature extraction by deep

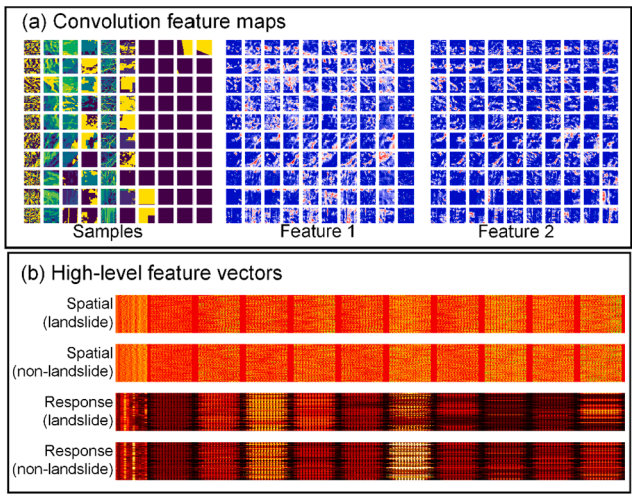

Fig. 11. The feature extraction process of SR. (a) Convolution feature maps in DSC layers. (b) High-level feature vectors of SPP layers.

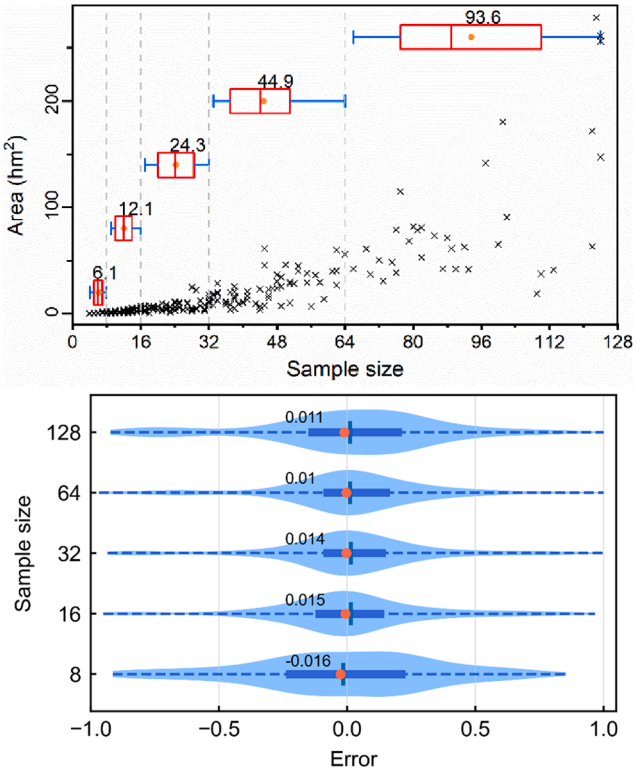

Fig. 12. Up: Distribution of landslides and corresponding sample size. Down: Errors of true values and predicted values under different sizes of samples.

learning, the ML classifiers work by the principle of partition data features (Merghadi et al., 2020), which has well interpretability and clear geoscience significance. The neural network implements through the logical regression layer, namely, the principle of error minimization, which considers the overall samples (Lecun et al., 2015; Li et al., 2018). However, ML cannot represent data features enough, especially when data increase and the features become complex. Visually, Fig. 11 shows the obvious difference of extracted features for landslide representation. Quantitatively, the experimental results (Table 3 and Fig. 10) also prove that the ML classifier has superiority in feature classification, except for the logical regression model. Therefore, our proposed method extracts high-level features by deep learning and adopts ML methods for feature classification. As shown in Figs. 8 and 9, the spatial prediction result of LSM conformed to the historical landslide distribution, and the result was more reliable and explainable.

6. Conclusions

In this study, we constructed a deep learning framework that combines spatial response features and ML classifier. In the Yarlung Zangbo Grand Canyon Region, 203 landslides and 11 conditioning factors were applied for performance evaluation. The factor analysis showed that distance factors (rivers and faults), NDVI, and rainfall have an obvious response to landslides. Compared with traditional ML models, accuracy analysis results indicated that our framework achieved the highest performance in terms of evaluation measures. Significantly, this study analyzed the extraction and utilization of high-level features by controlled experiments. The results revealed that our framework could effectively extract the spatial response features, and feature fusion from different directions can improve prediction accuracy. Moreover, for feature classification, ML classifiers were more effective than the FC layers with Sigmoid. Meanwhile, the framework can accept flexible input sizes for samples. The mean error indicated that suitable sample sizes while considering landslide scales performed better prediction ability.

In the future, our research will further explore the predisposing factors by considering weight analysis, and our prediction framework is expected to apply more effective deep learning architectures for LSM and risk management.

CRediT authorship contribution statement

Ruilong Wei: Methodology, Writing – original draft, Writing – review & editing, Software. **Chengming Ye:** Conceptualization, Writing – review & editing, Supervision, Funding acquisition. **Tianbo Sui:** Investigation, Visualization. **Yonggang Ge:** Writing – review & editing. **Yao Li:** Validation, Writing – review & editing. **Jonathan Li:** Writing – review & editing.

Declaration of Competing Interest

The authors declare that they have no known competing financial interests or personal relationships that could have appeared to influence the work reported in this paper.

Acknowledgments

This work was supported in part by the Second Tibetan Plateau Scientific Expedition and Research Program (STEP) under Grant 2019QZKK0902, the National Natural Science Foundation of China under Grant 42071411, the Strategic Priority Research Program of the Chinese Academy of Sciences under Grant XDA23090203, and the key research and development program of Sichuan Province (22ZDYF2824).

References

Achour, Y., Garçia, S., Cavaleiro, V., 2018. GIS-based spatial prediction of debris flows using logistic regression and frequency ratio models for Zêzere River basin and its surrounding area, Northwest Covilhã. Portugal. Arab. J. Geosci. 11, 1–17. https://doi.org/10.1007/S12517-018-3920-9.

Achour, Y., Pourghasemi, H.R., 2020. How do machine learning techniques help in increasing accuracy of landslide susceptibility maps? Geosci. Front. 11 (3), 871–883. https://doi.org/10.1016/j.gsf.2019.10.001.

Aditian, A., Kubota, T., Shinohara, Y., 2018. Comparison of GIS-based landslide susceptibility models using frequency ratio, logistic regression, and artificial neural network in a tertiary region of Ambon, Indonesia. Geomorphology 318, 101–111. https://doi.org/10.1016/j.geomorph.2018.06.006.

Anagnostopoulos, G.G., Fatichi, S., Burlando, P., 2015. An advanced process-based distributed model for the investigation of rainfall-induced landslides: The effect of process representation and boundary conditions. Water Resour. Res. 51 (9), 7501–7523. https://doi.org/10.1002/2015WR016909.

Arabameri, A., Saha, S., Roy, J., Chen, W., Blaschke, T., Tien Bui, D., 2020. Landslide Susceptibility Evaluation and Management Using Different Machine Learning Methods in The Gallicash River Watershed. Iran. Remote Sens. 12, 475. https://doi.org/10.3390/rs12030475.

Bojadjieva, J., Sheshov, V., Bonnard, C., 2018. Hazard and risk assessment of earthquake-induced landslides—case study. Landslides 15 (1), 161–171. https://doi.org/10.1007/s10346-017-0905-9.

Chen, C., Zhang, L., Xiao, T.e., He, J., 2020a. Barrier lake bursting and flood routing in the Yarlung Tsangpo Grand Canyon in October 2018. J. Hydrol. 583, 124603. https://doi.org/10.1016/j.jhydrol.2020.124603.

Chen, W., Peng, J., Hong, H., Shahabi, H., Pradhan, B., Liu, J., Zhu, A.X., Pei, X., Duan, Z., 2018. Landslide susceptibility modelling using GIS-based machine learning techniques for Chongren County, Jiangxi Province, China. Sci. Total Environ. 626, 1121–1135. https://doi.org/10.1016/j.scitotenv.2018.01.124.

Chen, W., Pourghasemi, H.R., Panahi, M., Kornejady, A., Wang, J., Xie, X., Cao, S., 2017a. Spatial prediction of landslide susceptibility using an adaptive neuro-fuzzy inference system combined with frequency ratio, generalized additive model, and support vector machine techniques. Geomorphology 297, 69–85. https://doi.org/10.1016/j.geomorph.2017.09.007.

Chen, W., Xie, X., Wang, J., Pradhan, B., Hong, H., Bui, D.T., Duan, Z., Ma, J., 2017b. A comparative study of logistic model tree, random forest, and classification and regression tree models for spatial prediction of landslide susceptibility. CATENA 151, 147–160. https://doi.org/10.1016/j.catena.2016.11.032.

Chen, Y., Ming, D., Ling, X., Lv, X., Zhou, C., 2021. Landslide Susceptibility Mapping Using Feature Fusion-Based CPCNN-ML in Lantau Island, Hong Kong. IEEE J. Sel. Top. Appl. Earth Obs. Remote Sens. 14, 3625–3639. https://doi.org/10.1109/JSTARS.2021.3066378.

Chen, Y., Wei, Y., Wang, Q., Chen, F., Lu, C., Lei, S., 2020b. Mapping post-earthquake landslide susceptibility: A U-net like approach. Remote Sens. 12, 2767. https://doi.org/10.3390/RS12172767.

Chollet, F., 2017. Xception: Deep learning with depthwise separable convolutions. In: Proceedings - 30th IEEE Conference on Computer Vision and Pattern Recognition, CVPR 2017. Institute of Electrical and Electronics Engineers Inc., pp. 1800–1807. https://doi.org/10.1109/CVPR.2017.195

Clerici, A., Perego, S., Tellini, C., Vescovi, P., 2006. A GIS-based automated procedure for landslide susceptibility mapping by the Conditional Analysis method: The Baganza valley case study (Italian Northern Apennines). Environ. Geol. 50 (7), 941–961. https://doi.org/10.1007/s00254-006-0264-7.

Dagdelenler, G., Nefeslioglu, H.A., Gokceoglu, C., 2016. Modification of seed cell sampling strategy for landslide susceptibility mapping: an application from the Eastern part of the Gallipoli Peninsula (Canakkale, Turkey). Bull. Eng. Geol. Environ. 75 (2), 575–590. https://doi.org/10.1007/s10064-015-0759-0.

Dao, D.V., Jaafari, A., Bayat, M., Mafi-Gholami, D., Qi, C., Moayedi, H., Phong, T.V., Ly, H.-B., Le, T.-T., Trinh, P.T., Luu, C., Quoc, N.K., Thanh, B.N., Pham, B.T., 2020. A spatially explicit deep learning neural network model for the prediction of landslide susceptibility. CATENA 188, 104451. https://doi.org/10.1016/j.catena.2019.104451.

Delaney, K.B., Evans, S.G., 2015. The 2000 Yigong landslide (Tibetan Plateau), rockslide-dammed lake and outburst flood: Review, remote sensing analysis, and process modelling. Geomorphology 246, 377–393. https://doi.org/10.1016/j.geomorph.2015.06.020.

Du, G., Zhang, Y., Yang, Z., Guo, C., Yao, X., Sun, D., 2019. Landslide susceptibility mapping in the region of eastern Himalayan syntaxis, Tibetan Plateau, China: a comparison between analytical hierarchy process information value and logistic regression-information value methods. Bull. Eng. Geol. Environ. 78 (6), 4201–4215. https://doi.org/10.1007/s10064-018-1393-4.

Fan, X., Scaringi, G., Korup, O., West, A.J., Westen, C.J., Tanyas, H., Hovius, N., Hales, T. C., Jibson, R.W., Allstadt, K.E., Zhang, L., Evans, S.G., Xu, C., Li, G., Pei, X., Xu, Q., Huang, R., 2019. Earthquake-Induced Chains of Geologic Hazards: Patterns, Mechanisms, and Impacts. Rev. Geophys. 57 (2), 421–503. https://doi.org/10.1029/2018RG000626.

Fang, Z., Wang, Y., Peng, L., Hong, H., 2020. Integration of convolutional neural network and conventional machine learning classifiers for landslide susceptibility mapping. Comput. Geosci. 139, 104470. https://doi.org/10.1016/j.cageo.2020.104470.

Ghorbanzadeh, O., Blaschke, T., Gholamnia, K., Meena, S., Tiede, D., Aryal, J., 2019a. Evaluation of Different Machine Learning Methods and Deep-Learning Convolutional Neural Networks for Landslide Detection. Remote Sens. 11, 196. https://doi.org/10.3390/rs11020196.

Ghorbanzadeh, O., Meena, S.R., Blaschke, T., Aryal, J., 2019b. UAV-based slope failure detection using deep-learning convolutional neural networks. Remote Sens. 11, 2046. https://doi.org/10.3390/rs11172046.

Gorum, T., Fan, X., van Westen, C.J., Huang, R.Q., Xu, Q., Tang, C., Wang, G., 2011. Distribution pattern of earthquake-induced landslides triggered by the 12 May 2008 Wenchuan earthquake. Geomorphology 133 (3-4), 152–167. https://doi.org/10.1016/j.geomorph.2010.12.030.

Guo, C., Montgomery, D.R., Zhang, Y., Wang, K., Yang, Z., 2015. Quantitative assessment of landslide susceptibility along the Xianshuihe fault zone, Tibetan Plateau, China. Geomorphology 248, 93–110. https://doi.org/10.1016/j.geomorph.2015.07.012.

Guo, Y., Ge, Y., Cui, P., Chen, X., Mao, P., Liu, T., Zhou, L., 2021. Early and mid-Holocene hydroclimate change recorded in tufa deposits in the Jiuzhaigou gully, eastern Tibetan Plateau. CATENA 196, 104834. https://doi.org/10.1016/j.catena.2020.104834.

Guzzetti, F., Mondini, A.C., Cardinali, M., Fiorucci, F., Santangelo, M., Chang, K.-T., 2012. Landslide inventory maps: New tools for an old problem. Earth-Science Rev. 112, 42–66. https://doi.org/10.1016/j.earscirev.2012.02.001.

He, K., Zhang, X., Ren, S., Sun, J., 2015. Spatial pyramid pooling in deep convolutional networks for visual recognition. IEEE Trans. Pattern Anal. Mach. Intell. 37 (9), 1904–1916. https://doi.org/10.1109/TPAMI.2015.2389824.

He, Q., Shahabi, H., Shirzadi, A., Li, S., Chen, W., Wang, N., Chai, H., Bian, H., Ma, J., Chen, Y., Wang, X., Chapi, K., Ahmad, B.B., 2019. Landslide spatial modelling using novel bivariate statistical based Naive Bayes, RBF Classifier, and RBF Network machine learning algorithms. Sci Total Env. 663, 1–15. https://doi.org/10.1016/j.scitotenv.2019.01.329.

He, Y., Zhao, Z., Yang, W., Yan, H., Wang, W., Yao, S., Zhang, L., Liu, T., 2021. A unified network of information considering superimposed landslide factors sequence and pixel spatial neighbourhood for landslide susceptibility mapping. Int. J. Appl. Earth Obs. Geoinf. 104, 102508. https://doi.org/10.1016/j.jag.2021.102508.

Hong, H., Pradhan, B., Xu, C., Tien Bui, D., 2015. Spatial prediction of landslide hazard at the Yihuang area (China) using two-class kernel logistic regression, alternating decision tree and support vector machines. CATENA 133, 266–281. https://doi.org/10.1016/j.catena.2015.05.019.

Hu, Q., Zhou, Y., Wang, S., Wang, F., 2020. Machine learning and fractal theory models for landslide susceptibility mapping: Case study from the Jinsha River Basin. Geomorphology 351, 106975. https://doi.org/10.1016/j.geomorph.2019.106975.

Huang, F., Yin, K., Huang, J., Gui, L., Wang, P., 2017. Landslide susceptibility mapping based on self-organizing-map network and extreme learning machine. Eng. Geol. 223, 11–22. https://doi.org/10.1016/j.enggeo.2017.04.013.

Huang, F., Zhang, J., Zhou, C., Wang, Y., Huang, J., Zhu, L., 2019. A deep learning algorithm using a fully connected sparse autoencoder neural network for landslide susceptibility prediction. Landslides 17 (1), 217–229. https://doi.org/10.1007/s10346-019-01274-9.

Huang, L., Luo, J., Lin, Z., Niu, F., Liu, L., 2020. Using deep learning to map retrogressive thaw slumps in the Beiluhe region (Tibetan Plateau) from CubeSat images. Remote Sens. Environ. 237, 111534. https://doi.org/10.1016/j.rse.2019.111534.

Huang, N., Lu, G., Xu, D., 2016. A permutation importance-based feature selection method for short-term electricity load forecasting using random forest. Energies 9, 767. https://doi.org/10.3390/en9100767.

Hungr, O., Leroueil, S., Picarelli, L., 2014. The Varnes classification of landslide types, an update. Landslides 11, 167–194. https://doi.org/10.1007/S10346-013-0436-Y/FIGURES/33.

Hussin, H.Y., Zumpano, V., Reichenbach, P., Sterlacchini, S., Micu, M., van Westen, C., Bălteanu, D., 2016. Different landslide sampling strategies in a grid-based bi-variate statistical susceptibility model. Geomorphology 253, 508–523. https://doi.org/10.1016/j.geomorph.2015.10.030.

Ji, S., Yu, D., Shen, C., Li, W., Xu, Q., 2020. Landslide detection from an open satellite imagery and digital elevation model dataset using attention boosted convolutional neural networks. Landslides 17 (6), 1337–1352. https://doi.org/10.1007/s10346-020-01353-2.

Jia, H., Chen, F., Pan, D., 2019. Disaster chain analysis of avalanche and landslide and the river blocking dam of the yarlung zangbo river in milin county of Tibet on 17 and 29 october 2018. Int. J. Environ. Res. Public Health 16, 4707. https://doi.org/10.3390/ijerph16234707.

Jibson, R.W., 2011. Methods for assessing the stability of slopes during earthquakes-A retrospective. Eng. Geol. 122 (1-2), 43–50. https://doi.org/10.1016/j.enggeo.2010.09.017.

Kavzoglu, T., Sahin, E.K., Colkesen, I., 2014. Landslide susceptibility mapping using GIS-based multi-criteria decision analysis, support vector machines, and logistic regression. Landslides 11 (3), 425–439. https://doi.org/10.1007/s10346-013-0391-7.

LeCun, Y., Bengio, Y., Hinton, G., 2015. Deep learning. Nature 521 (7553), 436–444. https://doi.org/10.1038/nature14539.

Lee, S., Pradhan, B., 2006. Landslide hazard mapping at Selangor, Malaysia using frequency ratio and logistic regression models. Landslides 4 (1), 33–41. https://doi.org/10.1007/s10346-006-0047-y.

Lei, T., Zhang, Y., Lv, Z., Li, S., Liu, S., Nandi, A.K., 2019. Landslide Inventory Mapping From Bitemporal Images Using Deep Convolutional Neural Networks. IEEE Geosci. Remote Sens. Lett. 16 (6), 982–986. https://doi.org/10.1109/LGRS.2018.2889307.

Li, Y., Cui, P., Ye, C., Junior, J.M., Zhang, Z., Guo, J., Li, J., 2021a. Accurate Prediction of Earthquake-Induced Landslides Based on Deep Learning Considering Landslide Source Area. Remote Sens. 13, 3436. https://doi.org/10.3390/rs13173436.

Li, Y., Zhang, H., Xue, X., Jiang, Y., Shen, Q., 2018. Deep learning for remote sensing image classification: A survey. WIREs Data Mining Knowl. Discov. 8 (6) https://doi.org/10.1002/widm.2018.8.issue-610.1002/widm.1264.

Li, Z., Chen, J., Han, M., Li, Y., Cao, C., Song, S., Zhang, Y., Yan, J., 2021b. Distribution and evolution of knickpoints along the Layue River. Eastern Himalayan Syntaxis. J. Hydrol. 603, 126915. https://doi.org/10.1016/j.jhydrol.2021.126915.

Luong, M.-T., Pham, H., Manning, C.D., 2015. Effective Approaches to Attention-based Neural Machine Translation. In: Conf. Proc. - EMNLP 2015 Conf. Empir. Methods Nat. Lang. Process, pp. 1412–1421. https://doi.org/10.18653/v1/d15-1166.

Girshick, R., 2015. Fast R-CNN. In: 2015 IEEE International Conference on Computer Vision (ICCV). pp. 1440–1448. https://doi.org/10.1109/ICCV.2015.169.

Ma, Y., Lu, M., Bracken, C., Chen, H., 2020. Spatially coherent clusters of summer precipitation extremes in the Tibetan Plateau: Where is the moisture from? Atmos. Res. 237, 104841. https://doi.org/10.1016/j.atmosres.2020.104841.

Marjanović, M., Kovačević, M., Bajat, B., Voženílek, V., 2011. Landslide susceptibility assessment using SVM machine learning algorithm. Eng. Geol. 123 (3), 225–234. https://doi.org/10.1016/j.enggeo.2011.09.006.

Merghadi, A., Yunus, A.P., Dou, J., Whiteley, J., ThaiPham, B., Bui, D.T., Avtar, R., Abderrahmane, B., 2020. Machine learning methods for landslide susceptibility studies: A comparative overview of algorithm performance. Earth-Science Rev. 207, 103225. https://doi.org/10.1016/j.earscirev.2020.103225.

Nefeslioglu, H.A., Gokceoglu, C., Sonmez, H., 2008. An assessment on the use of logistic regression and artificial neural networks with different sampling strategies for the preparation of landslide susceptibility maps. Eng. Geol. 97 (3-4), 171–191. https://doi.org/10.1016/j.enggeo.2008.01.004.

Park, I., Lee, S., 2014. Spatial prediction of landslide susceptibility using a decision tree approach: a case study of the Pyeongchang area, Korea. Int. J. Remote Sens. 35 (16), 6089–6112. https://doi.org/10.1080/01431161.2014.943326.

Park, S., Kim, J., 2019. Landslide Susceptibility Mapping Based on Random Forest and Boosted Regression Tree Models, and a Comparison of Their Performance. Appl. Sci. 9, 942. https://doi.org/10.3390/app9050942.

Pawluszek-Filipiak, K., Borkowski, A., 2020. On the importance of train-test split ratio of datasets in automatic landslide detection by supervised classification. Remote Sens. 12, 3054. https://doi.org/10.3390/rs12183054.

Pham, B.T., Tien Bui, D., Prakash, I., Dholakia, M.B., 2017. Hybrid integration of Multilayer Perceptron Neural Networks and machine learning ensembles for landslide susceptibility assessment at Himalayan area (India) using GIS. CATENA 149, 52–63. https://doi.org/10.1016/j.catena.2016.09.007.

Pourghasemi, H.R., Kornejady, A., Kerle, N., Shabani, F., 2020. Investigating the effects of different landslide positioning techniques, landslide partitioning approaches, and presence-absence balances on landslide susceptibility mapping. CATENA 187, 104364. https://doi.org/10.1016/j.catena.2019.104364.

Pourghasemi, H.R., Rahmati, O., 2018. Prediction of the landslide susceptibility: Which algorithm, which precision? Catena 162, 177–192. https://doi.org/10.1016/j.catena.2017.11.022.

Sameen, M.I., Pradhan, B., Lee, S., 2020. Application of convolutional neural networks featuring Bayesian optimization for landslide susceptibility assessment. CATENA 186, 104249. https://doi.org/10.1016/j.catena.2019.104249.

Samia, J., Temme, A., Bregt, A., Wallinga, J., Guzzetti, F., Ardizzone, F., Rossi, M., 2016. Do landslides follow landslides? Insights in path dependency from a multi-temporal landslide inventory. Landslides 14 (2), 547–558. https://doi.org/10.1007/s10346-016-0739-x.

Sharma, S., Mahajan, A.K., 2019. A comparative assessment of information value, frequency ratio and analytical hierarchy process models for landslide susceptibility mapping of a Himalayan watershed. India. Bull. Eng. Geol. Environ. 78 (4), 2431–2448. https://doi.org/10.1007/s10064-018-1259-9.

Thi Ngo, P.T., Panahi, M., Khosravi, K., Ghorbanzadeh, O., Kariminejad, N., Cerda, A., Lee, S., 2021. Evaluation of deep learning algorithms for national scale landslide susceptibility mapping of Iran. Geosci. Front. 12 (2), 505–519. https://doi.org/10.1016/j.gsf.2020.06.013.

Tien Bui, D., Tuan, T.A., Klempe, H., Pradhan, B., Revhaug, I., 2016. Spatial prediction models for shallow landslide hazards: a comparative assessment of the efficacy of support vector machines, artificial neural networks, kernel logistic regression, and logistic model tree. Landslides 13 (2), 361–378. https://doi.org/10.1007/s10346-015-0557-6.

Varnes, D.J., 1978. Slope movement types and processes. Landslides Anal. Control. Transp. Res. board Spec. Rep. 176, 11–33.

Wang, W., He, Z., Han, Z., Li, Y., Dou, J., Huang, J., 2020. Mapping the susceptibility to landslides based on the deep belief network: a case study in Sichuan Province, China. Nat. Hazards 103 (3), 3239–3261. https://doi.org/10.1007/s11069-020-04128-z.

Wang, Y., Fang, Z., Hong, H., 2019. Comparison of convolutional neural networks for landslide susceptibility mapping in Yanshan County, China. Sci. Total Environ. 666, 975–993. https://doi.org/10.1016/J.SCITOTENV.2019.02.263.

Wei, X., Zhang, L., Luo, J., Liu, D., 2021. A hybrid framework integrating physical model and convolutional neural network for regional landslide susceptibility mapping. Nat. Hazards 109 (1), 471–497. https://doi.org/10.1007/s11069-021-04844-0.

Wu, C., Guo, Y., Su, L., 2021. Risk assessment of geological disasters in Nyingchi. Tibet. Open Geosci. 13, 219–232. https://doi.org/10.1515/GEO-2020-0208.

Xiao, L., Zhang, Y., Peng, G., 2018. Landslide Susceptibility Assessment Using Integrated Deep Learning Algorithm along the China-Nepal Highway. Sensors (Basel) 18, 4436. https://doi.org/10.3390/s18124436.

Xu, Q., Fan, X.-M., Huang, R.-Q., Westen, C.V., 2009. Landslide dams triggered by the Wenchuan Earthquake, Sichuan Province, south west China. Bull. Eng. Geol. Environ. 68 (3), 373–386. https://doi.org/10.1007/s10064-009-0214-1.

Yang, X., Liu, R., Yang, M., Chen, J., Liu, T., Yang, Y., Chen, W., Wang, Y., 2021. Incorporating landslide spatial information and correlated features among conditioning factors for landslide susceptibility mapping. Remote Sens. 13, 2166. https://doi.org/10.3390/rs13112166.

Ye, C., Li, Y., Cui, P., Liang, L.i., Pirasteh, S., Marcato, J., Goncalves, W.N., Li, J., 2019. Landslide Detection of Hyperspectral Remote Sensing Data Based on Deep Learning With Constrains. IEEE J. Sel. Top. Appl. Earth Obs. Remote Sens. 12 (12), 5047–5060. https://doi.org/10.1109/JSTARS.2019.2951725.

Ye, C., Wei, R., Ge, Y., Li, Y., Junior, J.M., Li, J., 2021. GIS-based spatial prediction of landslide using road factors and random forest for Sichuan-Tibet Highway. J. Mt. Sci. 2022, 1–16. https://doi.org/10.1007/S11629-021-6848-6.

Yi, Y., Zhang, Z., Zhang, W., Jia, H., Zhang, J., 2020. Landslide susceptibility mapping using multiscale sampling strategy and convolutional neural network: A case study in Jiuzhaigou region. CATENA 195, 104851. https://doi.org/10.1016/j.catena.2020.104851.

Yunus, A.P., Fan, X., Tang, X., Jie, D., Xu, Q., Huang, R., 2020. Decadal vegetation succession from MODIS reveals the spatio-temporal evolution of post-seismic landsliding after the 2008 Wenchuan earthquake. Remote Sens. Environ. 236, 111476. https://doi.org/10.1016/j.rse.2019.111476.

Zhang, L., Xiao, T., He, J., Chen, C., 2019. Erosion-based analysis of breaching of Baige landslide dams on the Jinsha River, China, in 2018. Landslides 16 (10), 1965–1979. https://doi.org/10.1007/s10346-019-01247-y.

Zhao, B., Li, W., Wang, Y., Lu, J., Li, X., 2019. Landslides triggered by the Ms 6.9 Nyingchi earthquake, China (18 November 2017): analysis of the spatial distribution and occurrence factors. Landslides 16 (4), 765–776. https://doi.org/10.1007/s10346-019-01146-2.

Zhao, B., Wang, Y., Li, W., Su, L., Lu, J., Zeng, L.u., Li, X., 2021. Insights into the geohazards triggered by the 2017 Ms 6.9 Nyingchi earthquake in the east Himalayan syntaxis, China. CATENA 205, 105467. https://doi.org/10.1016/j.catena.2021.105467.

Zhou, J.-W., Cui, P., Hao, M.-H., 2016. Comprehensive analyses of the initiation and entrainment processes of the 2000 Yigong catastrophic landslide in Tibet, China. Landslides 13 (1), 39–54. https://doi.org/10.1007/s10346-014-0553-2.